Materials Science-Poland, 35(1), 2017, pp. 6-13
http://www.materialsscience.pwr.wroc.pl/
DOI: 10.1515/msp-2017-0032

DE GRUYTER OPEN

Morphologies of nanostructured bismuth sulphide and Mn (II) doped bismuth sulphide nanoparticles: characterization and application

NISHANT ANASANE, RAKSHIT AMETA*

Department of Chemistry, PAHER University, Udaipur 313003 (Raj.), India

Different morphologies of bismuth sulphide (Bi_2S_3) nanoparticles (NPs) were synthesized at room temperature using wet chemical method. The properties of bismuth sulphide (Bi_2S_3) nanoparticles can be controlled by different amounts of Mn^{2+} dopant. The synthesized nanoparticles were characterized by several techniques, such as high resolution scanning electron microscopy (HR-SEM), X-ray diffraction (XRD), transmission electron microscopy (TEM), electron diffraction (ED), and energy dispersive X-ray spectroscopy (EDS). The nanoparticles (Bi_2S_3) were found to have excellent activity for the UV light assisted decolorization of methyl violet dye and also helped to speed up the redox reaction of $Fe(CN)_6^{3-}$ and $S_2O_3^{2-}$. The reactions were monitored through UV-Vis spectroscopy.

Keywords: *nanostructures; dopant; metals; semiconductors; catalytic properties; surface properties*

1. Introduction

Over the last few years, semiconductor nanoparticles (NPs) have received considerable attention due to their wide applications in optical and electronic devices [1–3]. Different shapes of semiconductor nanoparticles have attracted attention in last decades, due to their effect on their magnetic and catalytic properties [4, 5]. Bismuth sulfide (Bi_2S_3) is a semiconductor having a direct band gap (E_g) of 1.3 eV [6, 7]. Doping of semiconductor nanomaterials with transition metal is important because it influences the electrical, optical, catalytic, and magnetic properties of the host semiconductor [8]. It is believed that doping a suitable metal ion, such as Mn^{2+}, into a semiconductor host material reduces the band gap of the semiconductor, resulting in faster transition of electrons between the conduction and valence band, and due to this property, it has found many applications in nanoelectronic devices [9].

Size and morphology of nanoparticles can be changed by doping a suitable metal ion into semiconductor nanoparticles [10]. Morphology of nanoparticles also depends upon the temperature at which the reaction was carried out, solvents used in the synthesis and the time required to complete the reaction, but these methods are especially dependent on high temperature and pressure [11]. Different methods have been reported for preparing bismuth sulphide nanoparticles, such as sonochemical method [12], microwave irradiation [13, 14] and thermal evaporation [15]. However, these methods require very high temperature and long time. Being less toxic and harmless, bismuth and its compounds can be used in various fields of biological, cosmetic and medical industries [16].

In the present study, we report the synthesis of bismuth sulphide nanoparticles by simple wet chemical method and change in the morphology of Bi_2S_3NPs with the doping of Mn^{2+} metal ions. The change in morphology of Bi_2S_3NPs with Mn^{2+} dopant, caused by using polyoxyethylene 100 stearate (Myrj59) as a capping agent, has been observed. The catalytic properties of as-synthesized materials were evaluated by decolorization of methyl violet dye and from the electron transfer reaction between potassium ferricyanide (PFC) and sodium thiosulphate (STS).

*E-mail: rakshit_ameta@yahoo.in

2. Experimental

2.1. Materials

Bismuth nitrate, manganese acetate, polyoxyethylene 100 stearate (Myrj59), Na_2S (sodium sulphide), nitric acid, potassium ferricyanide (PFC), sodium thiosulfate (STS) and methyl violet were purchased from Sigma Aldrich. All the solutions were prepared using doubly distilled and demineralized water.

2.2. Methods

2.2.1. Synthesis of Mn^{2+} doped bismuth sulphide nanoparticles

Mn^{2+} doped Bi_2S_3 nanoparticles were synthesized through wet chemical method using bismuth nitrate as a source of bismuth metal, manganese acetate and sodium sulphide as sources of manganese ion and sulphur. Polyoxyethylene 100 stearate (Myrj59) acted as a stabilizing agent. Mn (10 %) doped Bi_2S_3NPs were synthesized by using bismuth nitrate (1.25 g) and manganese acetate (0.26 g) solution in nitric acid (20 mL). 2 g of polyoxyethylene 100 stearate (Myrj59) were dissolved in 30 mL of deionized water and stirred for half an hour to form a homogeneous solution. 1.3 g of Na_2S was dissolved in 10 mL of deionized water. Thereafter, Na_2S solution was added to the Myrj59 solution under stirring. To this mixture, bismuth nitrate and manganese acetate solution were added dropwise. The reaction mixture was stirred for 5 h. The resulting precipitate was separated by centrifugation at 10000 rpm for 10 min, washed with sodium hydroxide, ethanol, water and acetone, and dried at 60 °C to 70 °C to obtain Mn^{2+} doped Bi_2S_3 black powder. Similarly, for comparison Mn doped (5 %) and undoped Bi_2S_3 nanoparticles were synthesized.

2.2.2. Characterization of Mn^{2+} doped Bi_2S_3 nanoparticles

X-ray powder diffraction (XRD) investigation was carried out on Shimadzu XRD-6000. The samples were prepared by pressing the dried powder and the patterns were collected with a scanning rate of 2°/min at 2θ ranging from 0° to 80°. The morphology of nanoparticles was examined by transmission electron microscopy (TEM). TEM images were recorded on Philips CM200 using an operating voltage of 200 kV. High resolution scanning electron microscopy investigation was done on FEI Quanta-FEG 200 (HR-SEM). Elemental composition was determined by energy dispersive X-ray (EDX) analysis of the vacuum dried doped and undoped Bi_2S_3 nanoparticles using a model JSM-5610 LV attached to scanning electron microscope (SEM). PerkinElmer Optima 4300 DV ICP-OES was used to analyze the constituents present in traces. FT-IR spectra were recorded for KBr pellet on the PerkinElmer Spectrum RX1 model in the range of 4000 cm^{-1} to 400 cm^{-1}. Doped and undoped Bi_2S_3 nanoparticles catalyzed decolorization of methyl violet dye and the redox reaction of $Fe(CN)_6^{3-}$ and $S_2O_3^{2-}$ were monitored by PerkinElmer LAMBDA 35 UV-Vis Spectrophotometer at corresponding λ_{max}. High pressure mercury vapor 125 W lamp (HPMV) was used as a source of UV light for dye reduction.

2.3. Decolorization of dye

The experiments were carried out using ethyl violet dye as a model system. Each UV light assisted reduction experiment was carried out by taking 25 mg Bi_2S_3 nanoparticles into a 250 mL glass UV chamber containing water jacket with 32.5×10^{-4} mol·L^{-1} of dye. Analogous experiments were performed with and without undoped Bi_2S_3 nanoparticles. The decolorization of the dye was measured by changes in its absorbance at λ_{max} using UV-Vis spectrophotometer.

2.4. Redox reaction

The reaction mixture containing as-synthesized Bi_2S_3 nanoparticles (7 mg), 1 mL of 0.001 mol potassium ferricyanide (PFC) and 1 mL of 0.1 mol sodium thiosulfate (STS) were placed in a quartz cell with 1 cm^3 path length. The reaction was monitored by UV-Vis spectrophotometer in the presence and absence of Bi_2S_3 NPs at 25±2 °C.

All experiments were repeated three times and the reproducibility was confirmed. The recyclability of the NPs was also studied. The NPs were recovered by centrifugation, washed with acetone,

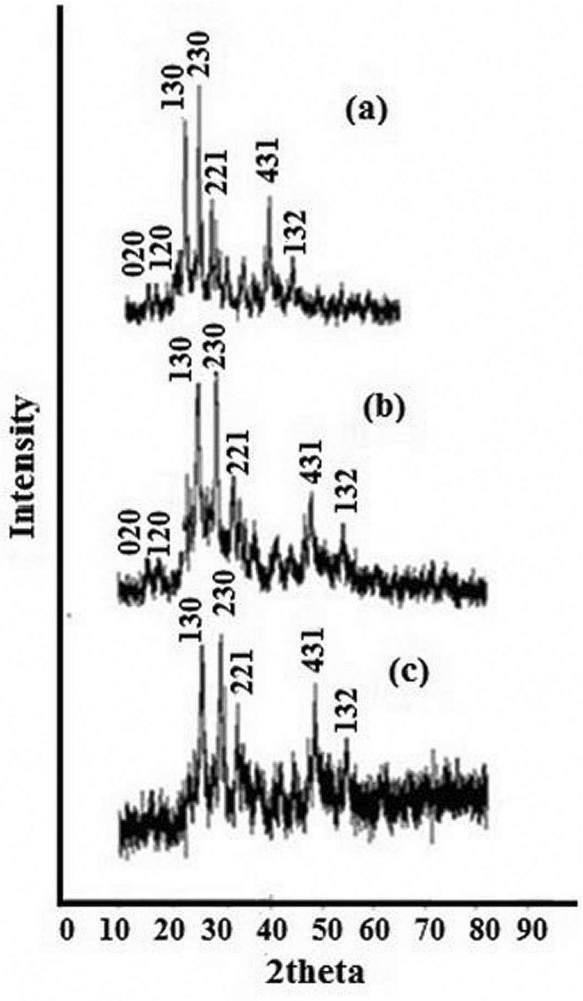

Fig. 1. XRD patterns of Bi_2S_3NPS (a)undoped, (b) doped with 5 % Mn ions and (c) doped with 10 % Mn ions.

dried at 60 °C under vacuum and used for the next reaction.

3. Results and discussion

3.1. XRD studies

Fig. 1 shows the XRD patterns of as-synthesized NPs. Fig. 1a is the XRD pattern of undoped Bi_2S_3NPs, whereas Fig. 1b and Fig. 1c show the spectra of 5 % and 10 % Mn ion doped Bi_2S_3NPs. Almost all peaks in the patterns could be indexed to a pure orthorhombic phase bismuth sulphide with the lattice parameters: a = 11.132 Å, b = 11.256 Å, and c = 3.976 Å, which is in a good agreement with the literature (JCPDS Card No. 17-320). The signals of Mn^{+2} were not detected in the XRD spectrum of bismuth sulphide. There were no other diffraction peaks which indicates high purity and crystalline nature of the nanoparticles.

The peak due to Bragg's reflection is observed at 2θ value corresponding to 25.3° and 28.9°. The particle size of undoped and Mn^{+2} doped Bi_2S_3 nanoparticles calculated from the Debye-Scherrer equation was 20±2 nm:

$$D = K\lambda/(\beta\cos\theta) \tag{1}$$

where K is the Scherrer constant, λ is the wavelength of the X-ray, β and θ are the half width of the peak at half of the Bragg angle, respectively.

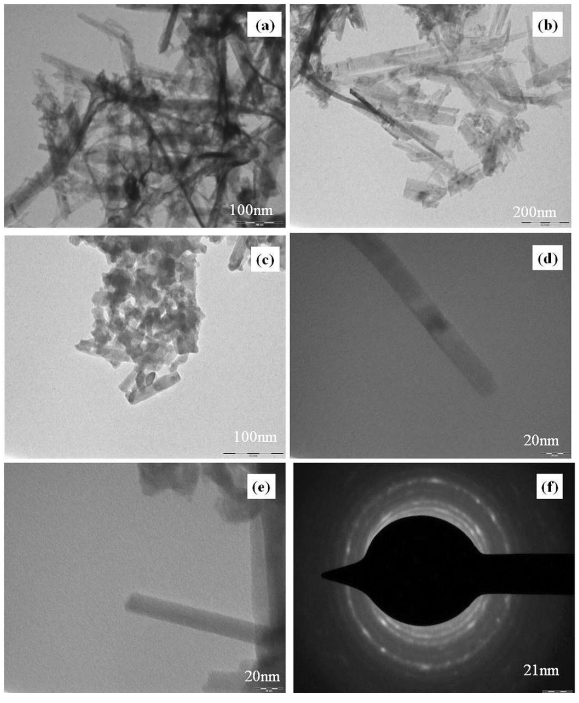

Fig. 2. TEM images of Bi_2S_3NPs (a) undoped, (b) doped with 5 % Mn ions and (c) doped with 10 % Mn ions, (d) and (e) TEM images at higher magnification, (f) ED pattern of Bi_2S_3NPs.

3.2. TEM analysis

The size and morphology of the Bi_2S_3 nanoparticles were analyzed by TEM. The TEM images

(Fig. 2) reveal that the undoped (Fig. 2a) and Mn^{+2} doped Bi_2S_3 nanoparticles consist of nanorods-like structures. When doping increased, the thickness of the rods also increased, as shown in Fig. 2b and Fig. 2c. Fig. 2d and Fig. 2e are TEM images of typical Bi_2S_3NPs at higher magnification. The diameter of the nanorods is in the range of 20 nm to 30 nm, and the length is about 200 nm to 250 nm. The observed rod type morphology of the product is probably due to chain type structure of bismuth sulphide. It is known that Bi_2S_3 molecules form band-like structures as Bi units are connected via weaker van der Waals forces [11]. It seems that the formation of Bi_2S_3NPs may have originated from the preferential directional growth of Bi_2S_3 crystallites. The crystallinity of the product was also proven by SAED (Fig. 2f).

3.3. HR-SEM analysis

Morphology of the product was also analyzed by HR-SEM. The HR-SEM images (Fig. 3) show the formation of bar-shaped nanorods of Bi_2S_3. Fig. 3a shows HR-SEM image of pure bismuth sulphide nanoparticles which look like bundles of thin nanorods. Fig. 3b shows HR-SEM image of Mn doped Bi_2S_3NPs (5 %) with thick nanorods. Fig. 3c shows cubic shaped Mn doped Bi_2S_3NPs (10 %). When Bi_2S_3 was doped with Mn^{2+} metal ions, the shape of Bi_2S_3NPs has also changed. Rod type morphology of bismuth sulphide may be due to the inherent chain type structure.

3.4. EDX analysis

The weight percentage of Mn^{2+} was determined by energy dispersive X-ray analysis (EDX) (Table 1, Fig. 4). EDX analysis indicates that the well-cleaned final product is mostly composed of Bi and S, with no other elements (Fig. 4a). Fig. 4b and Fig. 4c are EDX images of Mn^{2+} doped Bi_2S_3NPs with 5 % and 10 % doping of Mn ion, respectively.

3.5. FT-IR spectroscopy

The FT-IR spectra of Bi_2S_3NPs and pure polyoxyethylene 100 sterate (Myrj59) are given in Fig. 5. Both display the typical profile of C=O

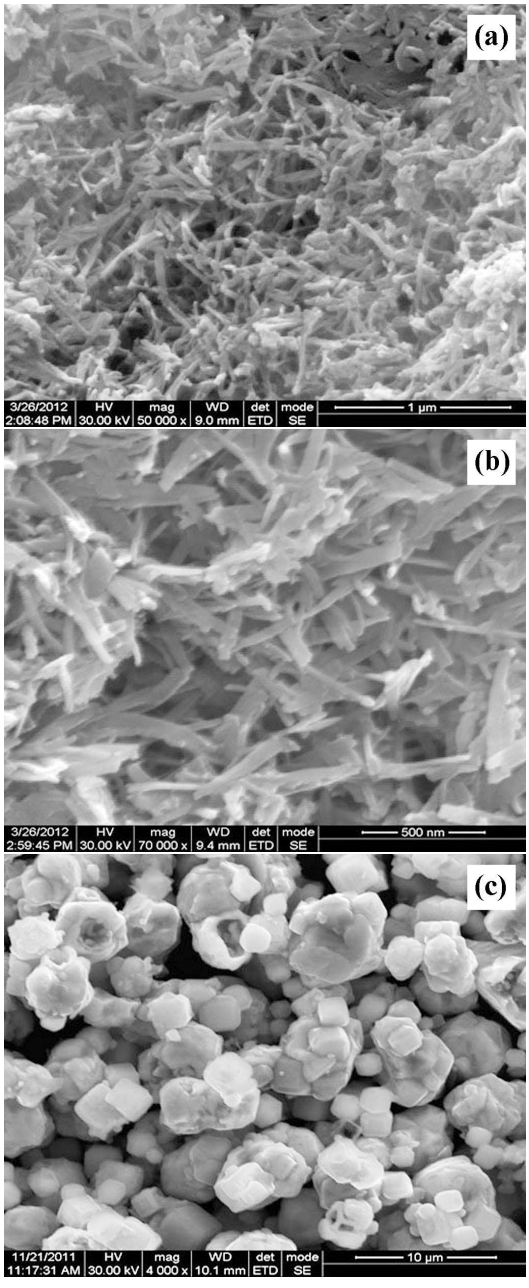

Fig. 3. HR-SEM images of (a) undoped Bi_2S_3 NPs, doped with (b) 5 % Mn ions and (c) 10 % Mn ions.

group of ester in the range of 1726 cm^{-1}. The peaks in the range of 1416 cm^{-1} to 1420 cm^{-1} are due to C–H bending. It is seen that the peak at 1726 cm^{-1} shifts to 1731 cm^{-1} in the Bi_2S_3NPs. The shifts observed in the spectra can be attributed to the interaction of Bi_2S_3NPs with the polyoxyethylene

Table 1. Percentage Mn (at.%, wt.%) as a dopant in Bi_2S_3 host determined by EDX, ICP.

Amount of Mn doped [at.%] used in synthesis	Actual amount of Mn in Bi_2S_3 matrix (from EDX) [%]	Mn/Bi [at.%] determined by ICP	Mn [wt.%] determined by ICP	Bi [wt.%] determined by ICP
0	–	–	–	–
5	3.5	4.8	3.62	56.24
10	8.2	9.3	9.47	50.57

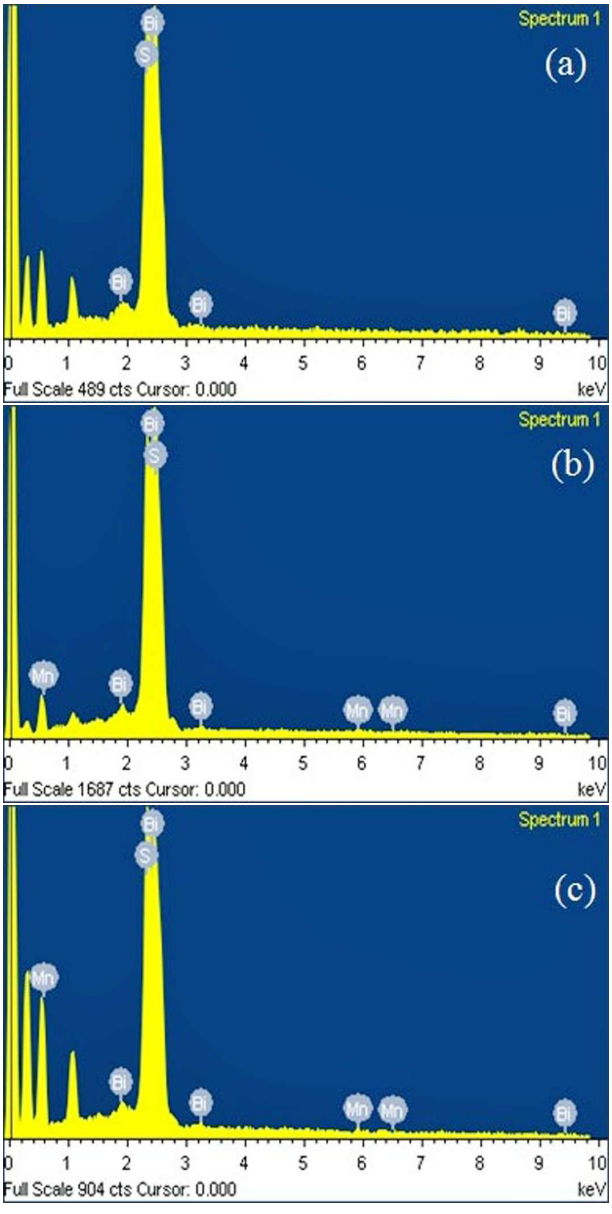

Fig. 4. EDX analysis of Bi_2S_3NPs (a) undoped and doped with (b) 5 % Mn ions and (c) 10 % Mn ions.

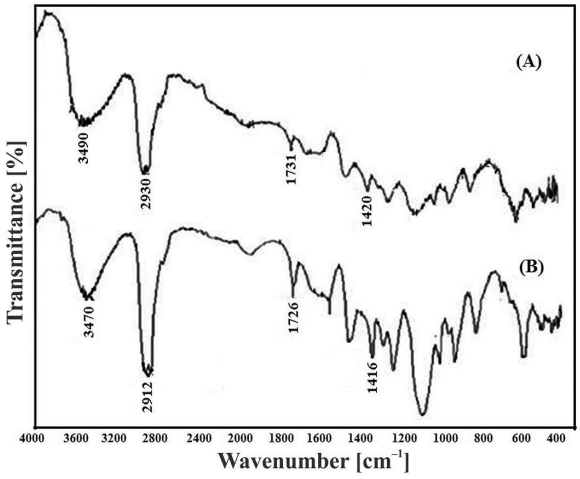

Fig. 5. FT-IR spectra of (A) Bi_2S_3NPs, (B) polyoxyethylene 100 sterate.

100 sterate. The band at 2912 cm^{-1} to 2930 cm^{-1} is characteristic of C–H stretching. The broad band due to hydrogen bonded hydroxyl group (O–H) appears in the range of 3470 cm^{-1} to 3490 cm^{-1} and it is attributed to the complex vibrational stretching, associated with free, inter and intra molecular bound hydroxyl groups.

3.6. Decolorization of methyl violet

Many industries, such as textile, paint, ink, plastics, cosmetics, etc., use a variety of dyes. Dyes are lost in a waste water stream during dyeing operation. The removal of the color of waste water is a burning issue all over the world, as it creates water pollution [17].

Various chemical methods, such as oxidation, precipitation, coagulation, etc., physical processes, such as adsorption, filtration, biological techniques, such as microbial degradation, etc., are used for

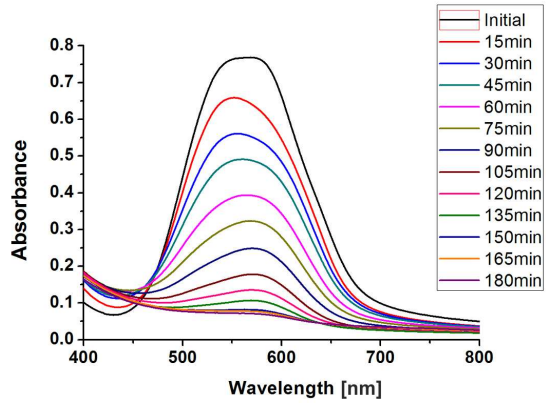

(a)

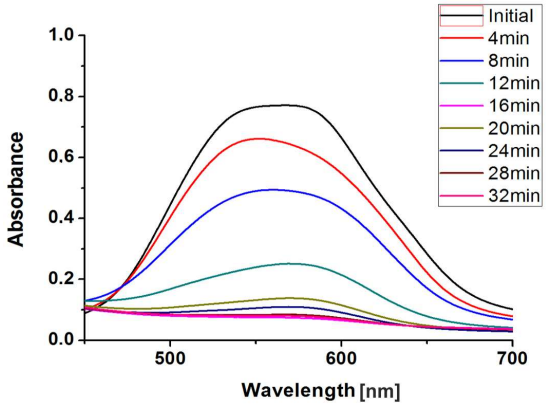

(b)

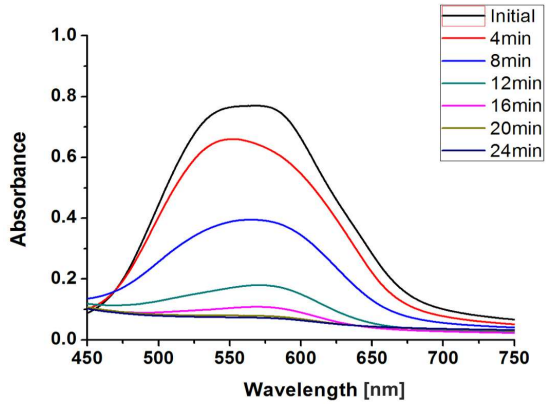

(c)

Fig. 6. UV-Vis spectra of methyl violet degradation (a) without NPs (b) with Mn doped (5 %) Bi_2S_3NPs (c) with Mn doped (10 %) Bi_2S_3NPs.

dye removal [18, 19]. Out of these, photocatalytic degradation process has been proven to be the most efficient way to decolor the dye effluents in an ecofriendly manner [20]. Photocatalytic degradation of pollutants by semiconductors is a new and effective technique for their removal from effluents of industries [21, 22]. Photocatalysis is defined as acceleration of a photochemical reaction in the presence of a catalyst.

In the present investigation, the photocatalytic decolorization of methyl violet dye has been carried out using undoped and Mn-doped Bi_2S_3NPs catalyst in a photoreactor. As a representative case, the catalytic activity of Bi_2S_3NPs was investigated in the decolorization of methyl violet dye. UV-Vis spectra in Fig. 6 show that before the addition of Bi_2S_3NPs, there was the maximum absorption band centered at 555 nm. UV light alone could not induce complete decolorization of the dye. But when irradiated in presence of Bi_2S_3NPs, UV light led to complete decolorization of the dye. The absorption band at 555 nm decreased and disappeared. When the size of bulk metals goes to the nanoscale, electron transfer is more efficient as compared to the bulk material [23, 24].

As shown in the UV-Vis spectra (Fig. 6) of methyl violet, without NPs photocatalytic decolorization did not take place completely even after 7 h. On the other hand, with NPs, the degradation was carried out in 180 min only. However, in the presence of 5 % and 10 % Mn doped Bi_2S_3NPs the degradation time was further reduced to 90 min (Fig. 6a) and 24 min (Fig. 6b), respectively.

The role of NPs in decolorization is as follows: when a photon of UV light strikes a surface of a semiconductor like Bi_2S_3NPs, a valence band electron moves to the conduction band, thus forming a positively charged hole in the valence band. The conduction band electrons and the valence band holes migrate then to the oxide surface and react with the chemisorbed O_2 or OH^-/H_2O molecules to generate reactive oxygen species, such as O_2^-, $HOO^{\cdot}$ and $^{\cdot}OH$ radicals which attack the dye molecules and cause their degradation [20, 24]. The mechanism for dye decolorization is similar to those discussed by Samira et al. [20] and Mohamed et al. [24].

Doping with a proper element is widely used as an effective method to tune surface states, energy

levels, electrical, optical, structural and magnetic properties of semiconductor materials [25–27].

To control the behavior of materials, doping is used, which lies at the heart of many technologies. For this reason, researchers have begun to explore the use of dopants to influence the properties of semiconductor nanoparticles [28]. The energy from absorbed photons can be efficiently transferred to the dopants which is utilized in the excitation and increases the rate of reactions on the surface of NPs [29]. Although the role of Myrj59 is only to cap the Bi_2S_3 NPs and to rule out the possibilities of decolorization by Myrj59, an experiment was performed with using it. No significant decrease in the absorbance was observed with using Myrj59.

3.7. Reaction between potassium ferricyanide and sodium thiosulfate

The electron transfer reaction between $Fe(CN)_6^{3-}$ and $S_2O_3^{2-}$ was catalyzed by a metal like Pt [30–32], Ni [33]. This reaction was performed for the first time in the presence of Bi_2S_3NPs. The characteristic absorption of $Fe(CN)_6^{3-}$ was observed at 420 nm. When reaction took place between $Fe(CN)_6^{3-}$ and $S_2O_3^{2-}$, the intensity of the corresponding peak (420 nm) decreased with time. In both the reactions, absorption was measured at time intervals of 3 min. In presence of Mn doped Bi_2S_3NPs (10 %) (Fig. 7a), there was a continuous decrease in absorbance at 420 nm with respect to time and after 24 min, the peak completely disappeared. In case of 5 % Mn doped Bi_2S_3 (Fig. 7b) completion of the reaction took 39 min. However, in the absence of Bi_2S_3 the reaction was proceeding very slowly and did not take place even after 6 h (Fig. 7c). On the basis of these observations it can be concluded that in presence of Bi_2S_3NPs, redox reactions proceed faster owing to efficient electron transfer due to the larger surface area of Bi_2S_3NPs.

4. Conclusions

Our experimental observations clearly indicate that Mn^{+2} doped Bi_2S_3 nanoparticles have been successfully synthesized using a simple wet

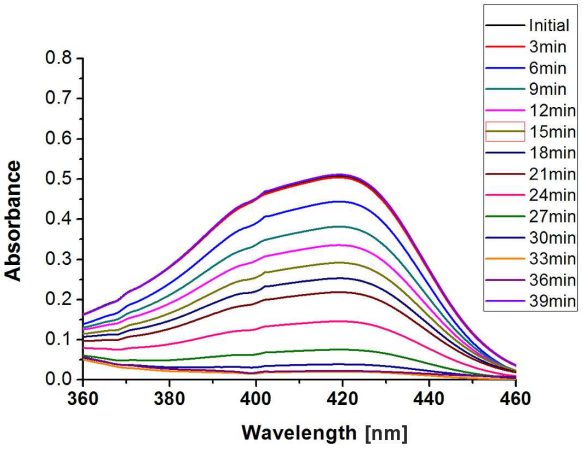

(a)

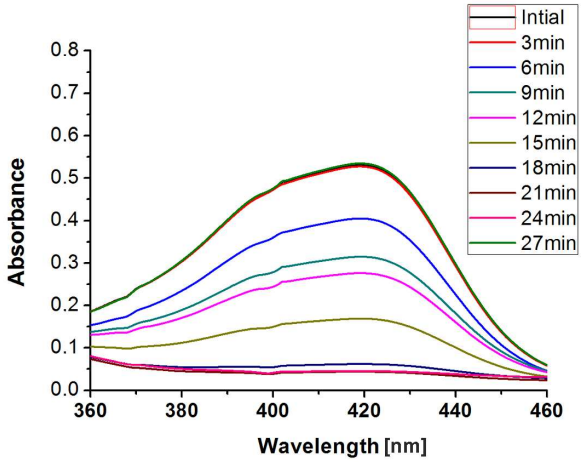

(b)

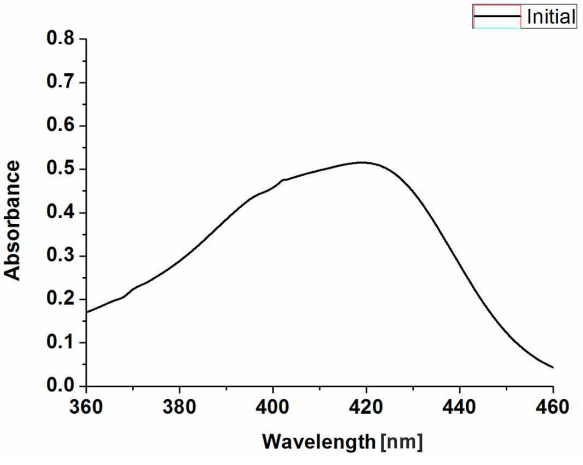

(c)

Fig. 7. UV spectra of redox reaction between $Fe(CN)_6^{3-}$ and $S_2O_3^{2-}$ (a) with Mn doped (10 %) Bi_2S_3NPs, (b) with Mn doped (5 %) Bi_2S_3NPs, (c) without Bi_2S_3NPs.

chemical method. The TEM study revealed that thin rod shaped NPs were obtained in cases of undoped Bi_2S_3NPs, while thick nanorods were formed in the presence of 5 % and 10 % Mn dopant ions. HR-SEM image also supported this observation. In HR-SEM images with 10 % loading of Mn dopant, NPs showed cubic shaped morphology. The present study allows us to conclude that multiple functionalities can be induced in NPs by doping or varying the dopant ion concentration. Further, Bi_2S_3NPs also helped in speeding up decolorization of methyl violet dye and changed the order of the redox reaction.

Acknowledgements

The Authors thank to the IIT Bombay and the IIT Madras for TEM, HR-SEM and EDX analysis.

References

[1] COLVIN V.L., SCHLAMP M.C., ALIVISATOS A.P., *Nature*, 370 (1994), 354.
[2] MANE R.M., MANE S.R., KHARADE R.R., BHOSALE P.N., *J. Alloy. Compd.*, 491 (2010), 321.
[3] MANEA R.M., GHANWATA V.B., KONDALKARA V.V., KHOTA K.V., MANEA S.R., PATILB P.S., BHOSALEA P.N., *ICMPC-2014*, 6 (2014), 1285.
[4] KRAHNE R., MANNA L., MORELLO G., FIGUEROLA A., GEORGE C., DEKA S., *Physical Properties of Nanorods*, Springer-Verlag, Berlin Heidelberg, 2013.
[5] PEREZ-JUSTE J., PASTORIA-SANTOS I., LIZ-MARZAN L.M., MULVANEY P., *Coord. Chem. Rev.*, 249 (2005), 1870.
[6] MURRAY C.B., KAGAN C.R., BAWENDI M.G., *Annu. Rev. Mater. Sci.*, 30 (2000), 545.
[7] ZHANG J.Z., *J. Phys. Chem. B*, 104 (2000), 7239.
[8] NAG A., CHAKRABORTY S., SARMA D.D., *J. Am. Chem. Soc.*, 130 (2008), 10605.
[9] DIXITA N., ANASANE N., CHAVDA M., BODAS D., SONI H.P., *Mater. Res. Bull.*, 48 (2013), 2259.
[10] GAO Y., CAO C., DAI L., LUO H., KANEHIRA M., DINGD Y., WANG Z.L., *Energ. Environ. Sci.*, 5 (2012), 8708.
[11] WANG H., ZHU J.J., ZHU J.M., CHEN H.Y., *J. Phys. Chem. B*, 106 (2002), 3848.
[12] WANG S.Y., DU Y.W., *J. Cryst. Growth*, 236 (2002), 627.
[13] LIAO X.H., WANG H., ZHU J.J., CHEN H.Y., *Mater. Res. Bull.*, 36 (2001), 2339.
[14] LIAO X.H., ZHU J.J., CHEN H.Y., *Mater. Sci. Eng. B-Adv.*, 85 (2001), 85.
[15] RINCON M.E., SANCHEZ M.P., GEORGE J., SANCHEZ A., NAIR P.K., *J. Solid State Chem.*, 136 (1998), 167.
[16] MOHAN R., *Nat. Chem.*, 2 (2010), 241.
[17] TEKBAS M., BEKTAS N., YATMAZ H.C., *Desalination*, 249 (2009), 205.
[18] KARTHIK V., SARAVANA K., BHARATHI P., DHARANYA V., MEIARAJ C., *JCHPS*, 7 (2014), 301.
[19] SARATALE R.G., SARATALE G.D., CHANG J.S., GOVINDWAR S.P., *J. Hazard. Mater.*, 166 (2009), 1421.
[20] SAMIRA S., RAJA A., MOHAN P., MODAK J.M., *J. Thermodyn. Catal.*, 3 (2012), 2157.
[21] MAHYAR A., BEHNAJADY M.A., MODIRSHAHLA N., *Photochem. Photobiol.*, 87 (2011), 795.
[22] SHIVARAJU H.P., *Int. J. Environ. Sci. Te.*, 5 (2011), 911.
[23] PANDE S., GHOSH S.K., NATH S., PRAHARAJ S., JANA S., PANIGRAHI S.J., *J. Colloid Interf. Sci.*, 299 (2006), 421.
[24] MOHAMED R.M., MCKINNEY D.L., SIGMUND W.M., *Mat. Sci. Eng. R*, 73 (2012), 1.
[25] CHEN Z., LI D., ZHANG W., SHAO Y., CHEN T., SUN M., FU X., *J. Phys. Chem. C*, 113 (2009), 4433.
[26] WANG X., SHEN S., JIN S., YANG J., LI M., WANG X., HANA H., LI C., *Phys. Chem. Chem. Phys.*, 15 (2013), 19380.
[27] JIA Y., SHEN S., WANG D., WANG X., SHI J., ZHANG F., HAN H., LI C., *J. Mater. Chem. A*, 1 (2013) 7905.
[28] ALIVISATOS A.P., *Science*, 271 (1996), 933.
[29] PRADHAN N., GOORSKEY D., THESSING J., PENG X.G., *J. Am. Chem. Soc.*, 127 (2005), 17586.
[30] NARAYANAN R., EL-SAYED M.A., *J. Phys. Chem. B*, 107 (2003), 12416.
[31] YANG W., MA Y., TANG J., YANG X., *Colloid. Surface. A*, 302 (2007), 628.
[32] PAL A., SHAH S., CHAKRABORTY D., DEVI S., *Aust. J. Chem.*, 61 (2008), 833.
[33] RATHORE P.S., RATHORE S., PATIDAR R., THAKORE S., *Catal. Lett.*, 144 (2014), 439.

Received 2016-05-07
Accepted 2017-01-21